

## Reynolds Pressure and Relaxation in a Sheared Granular System

Jie Ren, Joshua A. Dijksman, and Robert P. Behringer

*Department of Physics & Center for Non-linear and Complex Systems, Duke University,  
Science Drive, Durham, North Carolina 27708-0305, USA*

(Received 30 July 2012; published 2 January 2013)

We describe experiments that probe the evolution of shear jammed states, occurring for packing fractions  $\phi_S \leq \phi \leq \phi_J$ , for frictional granular disks, where above  $\phi_J$  there are no stress-free static states. We use a novel shear apparatus that avoids the formation of inhomogeneities known as shear bands. This fixed  $\phi$  system exhibits coupling between the shear strain,  $\gamma$ , and the pressure,  $P$ , which we characterize by the ‘‘Reynolds pressure’’ and a ‘‘Reynolds coefficient,’’  $R(\phi) = (\partial^2 P / \partial \gamma^2) / 2$ .  $R$  depends only on  $\phi$  and diverges as  $R \sim (\phi_c - \phi)^\alpha$ , where  $\phi_c \approx \phi_J$  and  $\alpha \approx -3.3$ . Under cyclic shear, this system evolves logarithmically slowly towards limit cycle dynamics, which we characterize in terms of pressure relaxation at cycle  $n$ :  $\Delta P \approx -\beta \ln(n/n_0)$ .  $\beta$  depends only on the shear cycle amplitude, suggesting an activated process where  $\beta$  plays a temperaturelike role.

DOI: [10.1103/PhysRevLett.110.018302](https://doi.org/10.1103/PhysRevLett.110.018302)

PACS numbers: 83.80.Fg, 62.20.D-, 83.85.Vb

Much recent work has focused on the mechanical behavior of disordered solids, including granular materials, colloids, foams, and molecular glass formers. These systems are well known for their glassy flow behavior and surprising rigidity. Notably, Bi *et al.* [1,2] recently showed that, in frictional systems, e.g., most common granular materials, shear strain,  $\gamma$ , can shear jam [2] a loose, low density packing of particles, enabling it to support a shear stress. The nature of these shear jammed states, particularly how they form and evolve, is an unsolved problem with obvious relevance, whose understanding is the goal of the current Letter.

To set the context, we note that Bi *et al.* [2] showed that there is a lowest packing fraction  $\phi_J$ , such that below (above) this density, there are (no) zero-stress states. Application of shear to a zero-stress state in  $\phi_S \leq \phi \leq \phi_J$  leads to highly anisotropic contact and force networks, to nonzero shear stress  $\tau$ , and to nonzero pressure  $P$ . Here,  $\tau = (\sigma_1 - \sigma_2) / 2$  and  $P = (\sigma_1 + \sigma_2) / 2$ , where the  $\sigma_i$  are the principal stresses of the 2D stress tensor,  $\hat{\sigma}$ . Starting from zero stress, the system traverses a fragile regime and, with additional shear strain, the system arrives at a fully jammed state where the force or contact networks percolate in all directions. These shear jammed states may occur naturally in many granular systems, such as geophysical flows, sand, and suspensions. Improved understanding of shear jammed states is thus crucial for both a better understanding of the concept of jamming for (frictional) materials and to shed light on the complex rheology of dense granular media [3].

At the heart of shear jamming are classic studies by Reynolds, who showed that, under fixed pressure, granular systems can dilate in response to shear [4]. Despite its relevance, a quantitative understanding of this effect has remained elusive over the last century. This is partly due to a complication in the study of sheared frictional materials: Shear typically induces the formation of dilated localized

shear bands, where most of the shear strain is confined. System-wide measures may tend to reflect the band properties rather than the whole system, making it difficult to interpret experiments.

To understand the important physics underlying shear jamming, it is crucial to have an experimental approach that avoids shear banding. In this Letter, we describe such an approach that, for the first time to our knowledge, avoids shear banding. Measurements using this method provide the first characterizations of, and key insights into, the mechanical response and dynamics of shear jammed frictional packings. In these fixed volume experiments, the response to shear is manifested as a nonlinearly growing pressure with shear strain, which is related to Reynolds’ dilatancy. Associated with this pressure effect are structural rearrangements that lead to a surprising Arrhenius-like stress relaxation dynamics in periodically sheared disk packings.

*Key findings.*—In these experiments, we shear a disordered disk packing (2D) at fixed density. In such a system, dilatancy cannot occur, but a related phenomenon occurs: The stresses  $\hat{\sigma}$  respond to the shear strain. We find that  $P$  increases roughly as  $\gamma^2$ , which we describe by a ‘‘Reynolds coefficient,’’  $R = (\partial^2 P / \partial \gamma_{1\phi}^2) / 2$ . We find that  $R$  depends only on  $\phi$  and it provides a simple parametrization of the coupling between  $P$  and  $\gamma$ .  $R$  seems to diverge as  $\phi$  approaches  $\phi_c \approx \phi_J$ , thus identifying a special role for  $\phi_J$  for the shear jamming states.

An additional key observation from this work is that for  $\phi_S \leq \phi \leq \phi_J$  the stress response to cyclic shear strain shows slow relaxational dynamics to a limit cycle that depends on driving. The deviation from a limit cycle, measured by pressure, shows a logarithmic decay over time or cycle number. The data for stress relaxation exhibit a totally unexpected scaling form, as developed below.

*Experimental setup.*—Key to these experiments is a novel apparatus that provides (simple) shear throughout

the system, in contrast to wall-driven shear. The base of the apparatus consists of narrow, parallel, horizontal, and transparent slats. Shear is applied by deforming the slats and boundary uniformly in the  $y$  direction, keeping the  $x$  dimension fixed at  $L$ , to provide uniform simple shear strain  $\gamma = \Delta y/L$  at constant packing fraction  $\phi$  [Fig. 1(a)]. On the slats rest  $\sim 1000$  bidisperse photoelastic particles (Vishay PSM-4) of diameters 12.7 and 15.9 mm; the slat width is of the order of the particle size. The relative numbers of large to small particles is set to 1:3.3, in order to prevent crystallization. Before each experiment, we prepare a stress-free packing by rearranging the particles (gently tapping or pushing particles) until no visual photoelastic response is visible. This bottom-assisted shear induces a linear shear profile, suppressing shear bands and the usual inhomogeneities. It is reminiscent of the SLLOD and related algorithms [5] for enforcing uniform shear in molecular dynamics simulations. It bears some resemblance to 3D experiments by Mueggenburg [6] but with a key difference: In the Mueggenburg experiments, a slat geometry was used, but the slot motion was not coordinated, and sustained uniform shear did not occur. We note that a small background pressure of  $\sim 0.5$  N/m is detected, even in the absence of shear. This is due to roughly equal amounts to small experimental errors in force determinations, our ability to completely relax all interparticle forces, and weak friction between the particles and the slats.

The experiment is illuminated from below by circularly polarized uniform white light and from above by a less intense UV light. A 22 megapixel camera above the experiment records views with and without a circular polarizer. We apply quasistatic shear strain in small steps. After each step, we pause and record three views of the system that respectively yield particle positions, photoelastic responses, and rotations. Without crossed polarizers, the edges of the particles are visible [Fig. 1(b), upper panel],

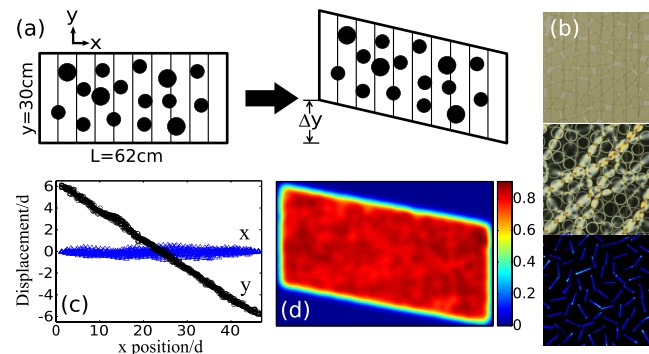


FIG. 1 (color online). (a) Setup schematics. (b) The three close-up images that the camera captures at each step: particle positions (upper), force response under polariscope (middle), and particle orientation images under UV light (lower). (c) The  $x$  and  $y$  displacements of particles vs their horizontal positions in the system. (d) The coarse-grained [12,13] density profile after 27% linear shear.

and we use a circular Hough-transform technique [7] to determine particle centers with an accuracy of  $\sim 0.02d$ . With a circular polarizer in front of the camera, we image the photoelastic pattern of colored or shaded fringes within each particle, which encode the contact forces acting on each particle [Fig. 1(b), middle panel]. To determine the particle orientations, each disk is marked diametrically with a line of fluorescent dye, visible under UV light with the white light turned off [Fig. 1(b), lower panel]. Changes in the bar orientations give particle rotations. The complete process of multiple strain steps, followed by imaging after each step, is fully automated, and we record up to 500 shear cycles per run. We extract the local particle stress by either a pattern-fitting approach [1,8], yielding the complete contact network, particle forces, and stress tensor (e.g.,  $P$  and  $\tau$ ), or, via  $G^2$ , the local squared intensity gradient of the photoelastic response, averaged on each particle [9,10].  $G^2$  is a one-to-one function of  $P$  on the particle level, providing an efficient measure for  $P$ . For small (large) data sets, we use the former (latter) approach.

*Reynolds effect.*—As noted, a striking aspect of applying shear strain to a stress-free state for  $\phi_S \leq \phi \leq \phi_J$  is the generation of nonzero  $P$  and  $\tau$ , as in the shear jamming experiments of Bi *et al.* [2]. In the present experiments, we go well beyond Bi *et al.* to probe the *evolution* of shear jammed states, first by forward shearing the system and then by shearing cyclically. Regarding forward shear, we prepared packings in a stress-free initial state, for  $0.691 \leq \phi \leq 0.816$ , where  $\phi_J = 0.835 \pm 0.005$  and  $\phi_S \approx 0.75$ . We then quasistatically shear the system by 200 small strain steps of 0.27%, up to a total strain of  $\gamma = 54\%$  [11]. These experiments show shear jamming [2], as expected, but, unlike previous experiments, particle tracking data [Fig. 1(c)] show that the shear is effectively linear and homogeneous across the entire system. Particle displacements and rotations relative to the uniform shear background are small. The locally coarse-grained density field [12,13] [Fig. 1(d)] shows no sign of a shear band or permanent inhomogeneities.

For the larger  $\phi$ 's considered here, we could not apply the full 54% strain because  $P$  became so large that the layer was unstable to out-of-plane buckling. If buckling occurred, we terminated the forward shear experiment. The forward shear results, Fig. 2(a), indicate that the shear-induced Reynolds pressure increases roughly as  $\gamma^2$  with a density-dependent prefactor that we characterize by the Reynolds coefficient,

$$R = (\partial^2 P / \partial \gamma^2_\phi) / 2. \quad (1)$$

For linear isotropic elastic materials, no coupling between shear strain and pressure is expected. But, as we apply shear, the system becomes increasingly anisotropic, so a  $P - \gamma$  coupling might be possible, as expressed by  $\partial P / \partial \gamma$ . In our system, this derivative grows roughly as  $\gamma$ , and linear elasticity is not a particularly useful concept.

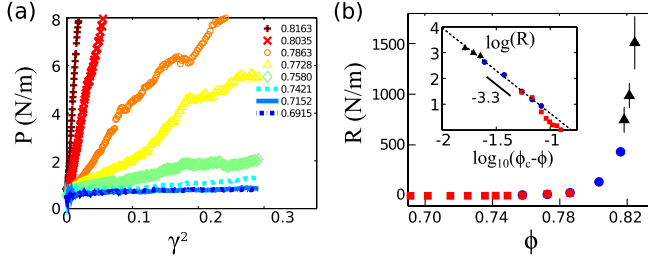


FIG. 2 (color online). (a) Reynolds pressure  $P(\gamma^2)$  observed in forward shear (see the text) tests for  $\phi = 0.691\text{--}0.816$ . (b) Reynolds coefficient  $R$  extracted from linear fitting, obtained from up to 54% forward shear (red squares), up to 27% forward shear (blue dots), and cyclic shear tests under limit cycle behavior (black triangles). The inset shows the same data on double logarithmic scales with  $\phi_c = 0.841 \pm 0.004$ . The error bar is smaller than the size of the symbols unless marked. The dashed line shows a fit to a power law. A line corresponding to an exponent  $-3.3$  is also shown for reference.

$R$  grows strongly with  $\phi$  and shows an apparent but unexpected divergence at  $\phi = \phi_c \approx \phi_J$ . Figure 2(b) and its inset show a log-log plot of  $R$  vs  $\Delta\phi = \phi_c - \phi$ . A power-law fit to  $R = A(\phi_c - \phi)^\alpha$  yields  $\alpha = -3.3 \pm 0.1$  and  $\phi_c = 0.841 \pm 0.004$ . By contrast,  $\phi_c$  lies in the range  $0.83 \leq \phi_j \leq 0.84$ , so here,  $\phi_c$  is not distinguishable from  $\phi_J$ , which is also comparable to  $\phi_J$  for systems of frictionless 2D particles. For  $\phi \leq 0.75$ , the system is very loose and it does not form a percolating contact network, even after 54% strain.  $R(\phi)$  behavior in this case is affected by small experimental “noise” effects, discussed above, and deviates from the power-law behavior [inset of Fig. 2(b)]. We identify  $\phi_S \approx 0.75$ , the lower limit in this system for shear jamming.

*Limit cycles.*—To characterize the evolution, reproducibility, and relaxation of the stresses, we carried out multiple shear cycles. This also allowed us to determine  $R$  for  $\phi$  closer to  $\phi_J$ , where shear strains are limited due to buckling; we obtain good statistics by many smaller-amplitude strain cycles. The oscillatory shear experiments were started from initially stress-free states for  $\phi$ 's in the shear jamming regime,  $\phi_S \leq \phi \leq \phi_J$ . In a cycle, we sheared by strain steps of 0.45% up to  $\gamma_{\max}$  in the “forward direction,” followed by a shear strain decrease ( $-0.45\%$  per step) to a smaller strain,  $\gamma_{\min}$ . For symmetric shear cycles,  $\gamma_{\min} = -\gamma_{\max}$ , and, for asymmetric shear cycles,  $\gamma_{\min} \neq -\gamma_{\max}$ .

For symmetric cycles,  $P$  was symmetric about  $\gamma = 0$ , approximately quadratic in  $\gamma$ , and virtually reproducible over many cycles, as shown in Fig. 3(a). However, details of the network were generally not reproducible from cycle to cycle. The Reynolds coefficient  $R(\phi)$  followed the same trend as in the forward shear tests [Fig. 2(b)], further confirming the Reynolds effect. After transients, the shear stress  $\tau$  also followed a reproducible path over cycles but, unlike  $P$ ,  $\tau$  was strongly hysteretic, with nonzero values at  $\gamma = 0$ . There were  $\gamma$ 's for which  $\tau = 0$  but  $P \neq 0$ , for

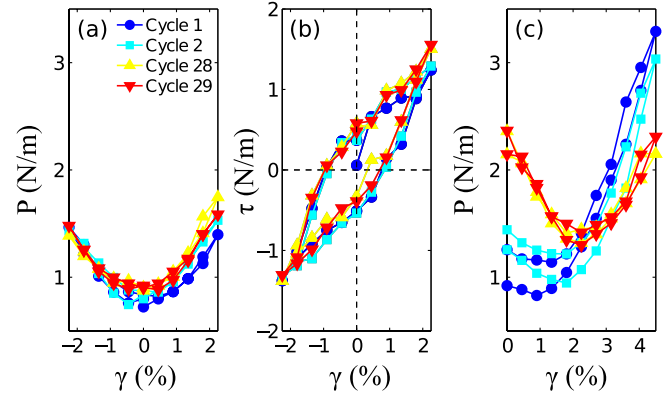


FIG. 3 (color online). (a)  $P$  vs  $\gamma$  for a symmetric cyclic shear run with  $\phi = 0.825$ , which started from  $\gamma = 0$  and sheared between  $\gamma_{\max} = 2.25\%$  and  $\gamma_{\min} = -2.25\%$ . Only cycles 1, 2, 28, and 29 are shown in the plot. (b)  $\tau$  vs  $\gamma$  for the same run and the same shear cycles. (c)  $P$  vs  $\gamma$  at cycles 1, 2, 28, and 29 for a nonsymmetric cyclic shear run ( $\gamma_{\max} = 4.5\%$ ,  $\gamma_{\min} = 0$ ) with the same density.

example, in Figs. 3(a) and 3(b) at  $\gamma \approx 1\%$ . However, in such cases,  $\tau$  coarse grained at smaller scales than the system size was *locally* nonzero, even though the global  $\tau$  was 0 (e.g., because of spatial variations of the principal stress orientations). Because of length limitations, we consider only the dynamics exhibited by  $P$  and we will present the full stress dynamics elsewhere.

The evolution of  $P(\gamma)$  for asymmetric shear cycles differed from the symmetric case. Here,  $P(\gamma)$  was initially asymmetric but evolved toward a symmetric shape centered around the mean strain,  $\bar{\gamma}$ , after many cycles. Thus, the long-term  $P - \gamma$  dynamics was a limit cycle. The system relaxed quickly (slowly) to the limit cycle if sheared symmetrically (asymmetrically). Figure 3(c) shows an example of slow evolution, where a limit cycle was reached after about 28 cycles. In this case,  $P(\gamma)$  evolved to a symmetric shape, similar to the forward shear experiment, except for a shift; i.e., the system did not reach a completely stress-free state at the midpoint of strain. However, a long-term limit cycle was still reached with the same Reynolds coefficient for the given density,  $\phi = 0.825$ .

*Slow relaxation.*—For asymmetric strain cycles,  $\Delta P(n) = P(\gamma_{\max}) - P(\gamma_{\min})$  was initially nonzero but it decreased and ultimately vanished, within fluctuations, for  $n = n_0$ . When the limit cycle was reached,  $P$  was symmetric about  $\bar{\gamma} = (\gamma_{\max} + \gamma_{\min})/2$ . The slow relaxation of  $\Delta P$  for asymmetric shear shows striking and novel scaling behavior, which we characterize in terms of  $\phi$ ,  $\bar{\gamma}$ , and the shear amplitude  $\gamma_A$ . Experiments to characterize this relaxation spanned  $\phi$ 's from above  $\phi_S$  to just below isotropic jamming  $\phi_J$ :  $0.780 \leq \phi \leq 0.828$ ; strain amplitudes of  $\gamma_A = 6.75\%$ ,  $4.5\%$ ,  $3\%$ , and  $1.5\%$ ; and a range of starting strains  $0 \leq \bar{\gamma} \leq 21.35\%$ . Experiments were 100–500 cycles long; for convenience, we measured  $G^2$  only at

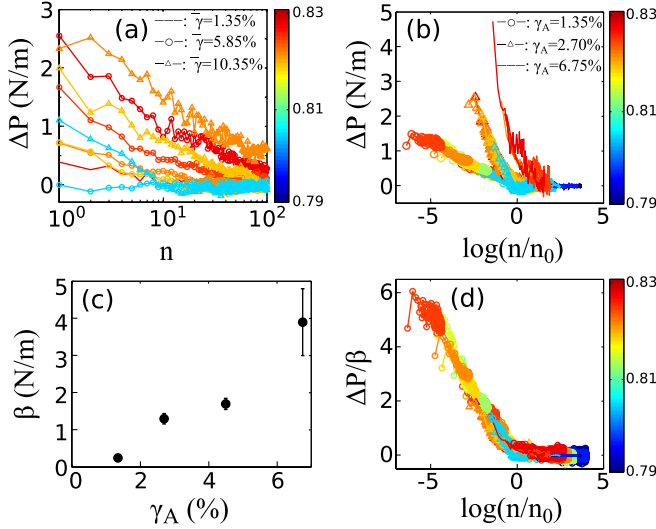


FIG. 4 (color online). (a)  $\Delta P$  vs number of shear cycles for various runs with  $\gamma_A = 2.7\%$  and  $\bar{\gamma} = 1.35\%$  (solid line),  $5.85\%$  (open circles), and  $10.35\%$  (open triangles). Different color or shading indicates different  $\phi$ . (b)  $\Delta P$  vs  $\log(n/n_0)$  for three different  $\gamma_A$ 's:  $1.35\%$  (open circles),  $2.70\%$  (open triangles), and  $6.75\%$  (solid lines). Data come from runs with various  $\phi$  (shown by color or shading) and various  $\bar{\gamma}$  (not shown). (c) The decay factor,  $\beta$ , shows a strong increase with  $\gamma_A$ . (d) The universal decay curve,  $\Delta P/\beta(\gamma_A)$  vs  $\log(n/n_0)$ , including all data from (b).

$\gamma_{\max}$ ,  $\gamma_{\min}$  and then converted  $G^2$  to  $\Delta P$  using a calibration. Figure 4(a) shows  $\Delta P$  for a particular  $\gamma_A$ .

For  $\phi$  in the shear jamming region,  $\Delta P(n)$  decayed logarithmically slowly towards 0:

$$\Delta P(n) \simeq -\beta \log(n/n_0), \quad (2)$$

implying a natural “time scale” for relaxation,  $n_0$ , that we obtained through least squares fits of the logarithmic part of the relaxation. All the relaxation data, for a given  $\gamma_A$ , collapse onto a single curve when expressed in terms of  $n/n_0$  [Fig. 4(b)], regardless of  $\phi$  and  $\bar{\gamma}$ . The factor  $\beta(\gamma_A)$  differs for each  $\gamma_A$  [Fig. 4(c)], but  $\Delta P/\beta$  is a universal function of  $n/n_0$ , as in Fig. 4(d), which shows all  $\sim 170$  data sets. We emphasize the remarkable role that  $\beta(\gamma_A)$  plays and the fact that it is independent of  $\phi$ .

We then consider what determines  $n_0$ . Equation (2) implies that  $n_0 = n \exp[\Delta P(n)/\beta(\gamma_A)]$ . Initially, at  $n = 1$ ,  $\Delta P = \Delta P_0$ . According to the approximately quadratic relation between  $P$  and  $\gamma$ ,  $\Delta P_0$  is given by  $\Delta P_0 = R(\phi)(\gamma_{\max}^2 - \gamma_{\min}^2)/2 = R(\phi)\bar{\gamma}\gamma_A$ . Therefore,

$$n_0 = \exp\left(R(\phi)\bar{\gamma}\frac{\gamma_A}{\beta(\gamma_A)}\right). \quad (3)$$

Equation (2) also implies an evolution  $d\Delta P/dn = -\beta n_0^{-1} \exp(\Delta P/\beta)$  or, with a cutoff,  $d\Delta P/dn = -\beta n_0^{-1} [\exp(\Delta P/\beta) - 1]$ , which produces the logarithmic form of Eq. (2) for small  $n$ , with saturation at  $n = n_0$ . This suggests an activated process, perhaps involving a

generalized ensemble, such as the stress ensemble, as discussed by several authors [14–17].

To summarize, for frictional granular systems in or near the shear jamming regime,  $\phi_S \leq \phi \leq \phi_J$ , we generated sheared states without shear bands, even with large strains or over many cycles of shear, making it possible to experimentally probe the constitutive relations of granular materials. These experiments show two key and highly novel results. (1) We find a novel Reynolds effect for fixed  $\phi$  that is approximately quadratic in  $\gamma$  using  $R = (\partial^2 P / \partial \gamma_{\phi}^2) / 2$ . We note that the specific form for  $R(\gamma)$  may well depend on the particle interaction force; a more general form might be  $P = R\gamma^\delta$ , where, for our experiments,  $\delta \simeq 2$ . (2) We find that, under cyclic shear, frictional granular systems evolve logarithmically slowly, as one might expect for an activated process, toward a state where the pressure is symmetric, *modulo* fluctuations, about the midpoint of strain. The pressure at the symmetry point may not be zero. This slow evolution is characterized by highly novel scaling behavior, such that there is good collapse of all data.

These results point toward several interesting directions. First, it is reasonable to search for a description of these states in terms of an ensemble picture, such as the stress ensemble, given the activated process character of the slow relaxation. Such a theory would need to explain some of the striking scaling properties observed here. In addition, we have not considered the properties of the shear stress under cyclic shearing, nor have we considered the particle dynamics of details of the force or contact networks. We will present these results elsewhere.

We thank Jie Zhang for sharing a code to perform rotational particle tracking. IGUS generously supplied us with a free linear stage under the Young Engineers Support Program. Discussions with Dapeng Bi, Bulbul Chakraborty, Martin van Hecke, Stefan Luding, and Corey O’Hern are gratefully acknowledged. Our work was supported by NSF Grants No. DMR-0906908 and No. DMR-1206351, ARO Grant No. W911NF-11-1-0110, and NSF Grant No. DMS0835742.

- [1] J. Zhang, T. Majmudar, A. Tordesillas, and R.P. Behringer, *Granular Matter* **12**, 159 (2010).
- [2] D. Bi, J. Zhang, B. Chakraborty, and R.P. Behringer, *Nature (London)* **480**, 355 (2011).
- [3] Y. Forterre and O. Pouliquen, *Annu. Rev. Fluid Mech.* **40**, 1 (2008).
- [4] O. Reynolds, *Philos. Mag.* **20**, 469 (1885).
- [5] D. J. Evans and G. P. Morriss, *Phys. Rev. A* **30**, 1528 (1984); P. Olsson and S. Teitel, *Phys. Rev. Lett.* **99**, 178001 (2007); D. J. Durian, *Phys. Rev. Lett.* **75**, 4780 (1995).
- [6] N. W. Mueggenburg, *Phys. Rev. E* **71**, 031301 (2005).
- [7] T. Peng, A. Balijepalli, S.K. Gupta, and T. LeBrun, *J. Comput. Inform. Sci. Eng.* **7**, 330 (2007).
- [8] T. S. Majmudar, M. Sperl, S. Luding, and R. P. Behringer, *Phys. Rev. Lett.* **98**, 058001 (2007).

- [9] D. Howell, R. P. Behringer, and C. Veje, *Phys. Rev. Lett.* **82**, 5241 (1999).
- [10] Junfei Geng, D. Howell, E. Longhi, R. P. Behringer, G. Reydellet, L. Vanel, E. Clément, and S. Luding, *Phys. Rev. Lett.* **87**, 035506 (2001).
- [11] J. Ren, J. A. Dijksman, and R. P. Behringer, *Chaos* **21**, 041105 (2011).
- [12] J. Zhang, R. P. Behringer, and I. Goldhirsch, *Prog. Theor. Phys. Suppl.* **184**, 16 (2010).
- [13] A. H. Clark, P. Mort, and R. P. Behringer, *Granular Matter* **14**, 283 (2012).
- [14] K. A. Reddy, Y. Forterre, and O. Pouliquen, *Phys. Rev. Lett.* **106**, 108301 (2011).
- [15] R. P. Behringer, D. Bi, B. Chakraborty, S. Henkes, and R. R. Hartley, *Phys. Rev. Lett.* **101**, 268301 (2008).
- [16] S. Henkes and B. Chakraborty, *Phys. Rev. Lett.* **95**, 198002 (2005); S. Henkes, C. S. O'Hern, and B. Chakraborty, *Phys. Rev. Lett.* **99**, 038002 (2007).
- [17] P. Sollich, F. Lequeux, P. Hébraud, and M. E. Cates, *Phys. Rev. Lett.* **78**, 2020 (1997); P. Sollich, *Phys. Rev. E* **58**, 738 (1998); P. Sollich and M. E. Cates, *Phys. Rev. E* **85**, 031127 (2012).